Plasmonic nanorods for enhanced absorption in mid-wavelength infrared detectors

M. Vallone*, M. Goano*†, A. Tibaldi*†, S. Hanna‡, D. Eich‡, A. Wegmann‡, H. Figgemeier‡
G. Ghione*, F. Bertazzi*†,
* Dipartimento di Elettronica e Telecomunicazioni, Politecnico di Torino, corso Duca degli Abruzzi 24, 10129 Torino, Italy
‡ AIM Infrarot-Module GmbH, Theresienstraße 2, D-74072 Heilbronn, Germany
† IEIIT-CNR, corso Duca degli Abruzzi 24, 10129 Torino, Italy
E-mail: michele.goano@polito.it

***Abstract*—The absorption properties of HgCdTe-based infrared detectors can be greatly increased in the mid-infrared band, by incorporating nanostructured plasmonic arrays on the illuminated detector face. The array periodicity, combined with the excitation of surface plasmon-polariton stationary modes, enhances the absorption efficiency by a substantial amount, allowing to reduce in turn the HgCdTe absorption thickness.**

I. Introduction

Dark current originating from lattice defects, thermal generation, radiative, and possibly tunneling processes limit the otherwise ideal HgCdTe (or MCT) performance, one of the most widely used materials for the fabrication of focal plane array (FPA) infrared (IR) detectors, extensively employed in IR cameras for scientific, civilian and defense purposes [1], [2]. Device cooling is an obvious remedy, but cost and weight constraints on the final product indicate the exactly opposite need. Immediate and popular alternatives are unipolar barrier detectors or fully depleted heterostructures [3], [4]. However, the former require non-trivial composition and doping profiles, the latter need high reverse bias to curtail dark current.

The reduction of the absorber thickness is surely helpful to minimize the dark current [5]–[7], but this inevitably reduces also the detector quantum efficiency (QE). In this regard, the adoption of periodic metallic nanostructures deposited on the detector illuminated face can be a viable solution [8]–[13] (see also Ref. [14] and references therein for a recent review). The general concept, the computational approach, and preliminary modeling results on MWIR (mid-wavelength IR, $\lambda \in [3, 5]\,\mu$m) detectors are presented in Section II, whereas an outlook on ongoing work is given in Section III.

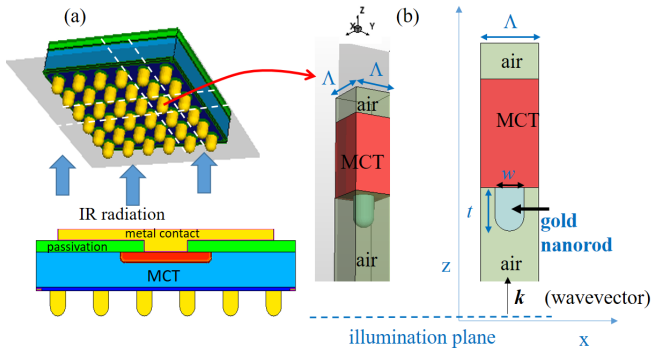

Fig. 1. (a) 3D MWIR FPA single pixel with nanorods on the illuminated face. The xz-cutplane at center pixel shows the epitaxial structure, the doping profile, the CdTe passivation layer, and the metallic bias contact. (b) One of the Λ-wide unit cells.

II. Plasmonic nanorods for MWIR detectors

Central concept is a two-dimensional (2D), Λ-periodic array of w-wide and t-long gold nanorods on the illuminated face of a FPA, which consists of a p-doped, t_{abs}-thick, planar $Hg_{0.7}Cd_{0.3}Te$ layer operating at $T = 230\,\text{K}$ (its cutoff wavelength is $\lambda_c \approx 4.5\,\mu$m). Pixels with a $3\,\mu$m pitch [15] are defined simulating a ion implantation which yields a n-p junction at $\approx 0.3\,\mu$m from the bias contact, and the illuminated face is located on the horizontal plane $z = 0$ (see Fig. 1). The FPA is illuminated from below with a monochromatic TE plane wave with electric field amplitude E_0 and wavevector along z. Convolutional perfectly matched layer (CPML) absorbing boundary conditions along z, and periodic boundary conditions (PBC) along x and y allow to consider just one of the pixels. Exploiting the periodicity of the structure, we can subdivide the pixel into Λ-wide square unit cells, each containing one of the nanorods. In these preliminary results, for the sake of simplicity, passivation and metallic contact are not included in the simulations, as it is shown in Fig. 1(b). PBC along x and y allow to simulate an infinitely extended 2D cells repetition: thus, the electromagnetic solution for one of the unit cells describes the whole pixel behavior.

The illumination triggers a collective surface plasmon-polariton mode along the nanorod-MCT interface. Its wavevector has a component in the horizontal plane given by $k_{\text{sp}}(\lambda) = 2\pi n_{\text{eff}}(\lambda)/\lambda$, where $n_{\text{eff}}^2 = \epsilon_{\text{Au}}\epsilon_{\text{MCT}}/(\epsilon_{\text{Au}} + \epsilon_{\text{MCT}})$. The λ-dependent ϵ_{Au} and ϵ_{MCT} are respectively the Au and MCT dielectric functions, which have been defined as in Ref. [16], [17]. The Λ-periodicity of the 2D nanorods distribution determines a

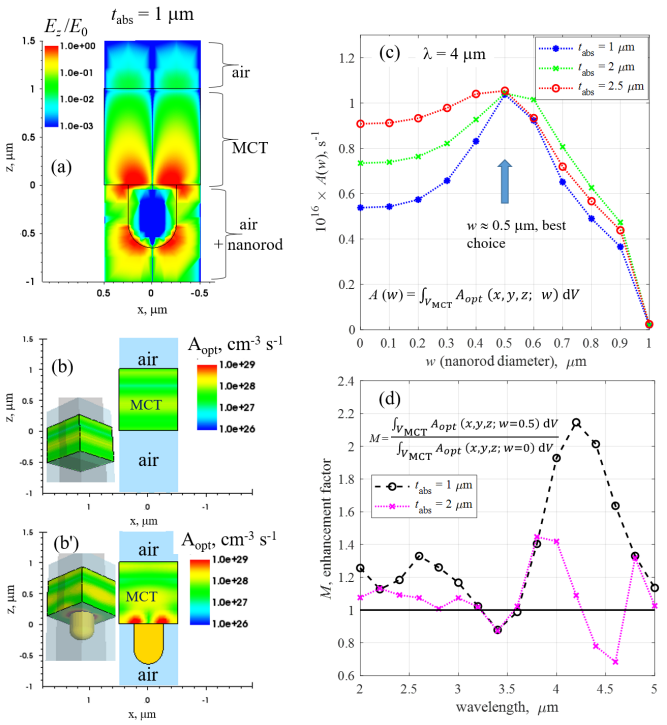

Fig. 2. For $\lambda = 4\,\mu$m, $t_{abs} = 1\,\mu$m: (a) the E_z distribution with nanorod (without it, of course it is $E_z = 0$); the absorbed photon density rate A_{opt}, without (b) and with (b') nanorod ($w = 0.5\,\mu$m); (c) A_{opt} integrated on the MCT volume vs. w; (d) the spectral absorption enhancement factor M, for $w = 0.5\,\mu$m.

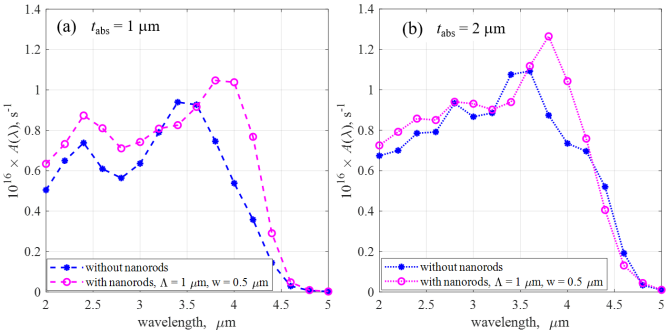

Fig. 3. The spectral absorbed photon density rate A_{opt} integrated on the MCT volume, without and with nanorods, for $t_{abs} = 1\,\mu$m (a) and $2\,\mu$m (b).

resonance condition given by $k_{sp}(\lambda) = (2\pi/\Lambda)\,(p\hat{x} + q\hat{y})$, where p and q are integers and $\hat{x}$, $\hat{y}$ are unit vectors (see Ref. [12] and references therein). As a first attempt, we set $\Lambda = 1\,\mu$m, which determines first order resonance for $\lambda \approx 3.5\,\mu$m, i.e., inside the MWIR band.

The electromagnetic problem is solved by a full-wave approach with Synopsys RSoft FullWAVE [18] according to the Finite Difference Time Domain (FDTD) method [19]. The nanorod length was fixed to $t = 0.4\,\mu$m, whereas the optimal nanorod diameter w was chosen by means of a series of three-dimensional FDTD simulations for $\lambda = 4\,\mu$m (center of the MWIR band), varying w in the interval $[0, \Lambda]$ (we remark that $w = 0$ identifies a standard absorber without nanorods). In Fig. 2 we show the effect of the nanorod on the electric field component E_z of the electromagnetic wave (a), and on the absorbed photon density rate A_{opt} (panels b, b'), for $\lambda = 4\,\mu$m, $t_{abs} = 1\,\mu$m, and $w = \Lambda/2$, since this value maximizes the absorption enhancement at MWIR center band, see Fig. 2(c). In Fig. 2(d) we show the *spectral* absorption enhancement factor M, still for $w = \Lambda/2$, whereas Fig. 3 shows the spectral rate A_{opt} integrated on the MCT volume, without and with nanorods, for $t_{abs} = 1\,\mu$m (a) and $2\,\mu$m (b). The nanorods effect is more evident for the thinnest absorber (see Fig. 3); moreover, Fig. 2(c) shows that a $1\,\mu$m thick MCT absorber with $w = \Lambda/2$ nanorods provides higher absorption than a $2.5\,\mu$m thick MCT absorber without nanorods ($w = 0$), making it unnecessary to consider $t_{abs} > 1\,\mu$m, to the potential benefit of reducing the dark current and increasing the detectivity [1, Eq. (1)].

III. Conclusion and future work

The calculated values of M potentially allow to employ thinner detectors, with great advantages in terms of dark current and inter-pixel crosstalk. Better targeted Λ and t optimizations are ongoing, in addition to multiphysics simulations of the complete pixel including electrical transport in order to quantify the effect of the nanorods on the spectral QE, following the approach outlined in Refs. [7], [13], [15], [20]–[22].

References

[1] P. Martyniuk, J. Antoszewski, M. Martyniuk, L. Faraone, A. Rogalski, *Appl. Phys. Rev.* **1**, 041102 (2014).
[2] R. K. Bhan, V. Dhar, *Opto-Electron. Rev.* **27**, 174 (2019).
[3] M. A. Kinch, *J. Electron. Mater.* **29**, 809 (2000).
[4] J. Schuster, R. E. DeWames, P. S. Wijewarnasurya, *J. Electron. Mater.* **46**, 6295 (2017).
[5] M. Vallone, *et al.*, *IEEE J. Electron Devices Soc.* **6**, 664 (2018).
[6] M. Vallone, *et al.*, *Appl. Opt.* **59**, E1 (2020).
[7] M. Vallone, *et al.*, *Opt. Quantum Electron.* **52**, 25 (2020).
[8] J. Liang, W. D. Hu, X. S. Chen, Z. F. Li, W. Lu, *20th International Conference on Numerical Simulation of Optoelectronic Devices (NUSOD 2020)* (Palma de Mallorca, Spain, 2014), pp. 179–180.
[9] M. Malerba, *et al.*, *Sci. Rep.* **5**, 16436 (2015).
[10] Y. Zhong, S. D. Malagari, T. Hamilton, D. Wasserman, *J. Nanophoton.* **9**, 093791 (2015).
[11] K. Tappura, *MDPI Proc.* **2**, 1063 (2018).
[12] N. Vanamala, K. C. Santiago, N. C. Das, *AIP Adv.* **9**, 025113 (2019).
[13] N. Vanamala, K. C. Santiago, N. C. Das, S. K. Hargrove, *AIP Adv.* **10**, 065006 (2020).
[14] N. Anttu, *et al.*, *J. Appl. Phys.* **129**, 131102 (2021).
[15] M. Vallone, *et al.*, *J. Electron. Mater.* **46**, 5458 (2017).
[16] M. A. Ordal, *et al.*, *Appl. Opt.* **22**, 1099 (1983).
[17] C. A. Hougen, *J. Appl. Phys.* **66**, 3763 (1989).
[18] Synopsys, Inc., Inc., Optical Solutions Group, Ossining, NY, *RSoft FullWAVE User Guide, v2017.03* (2017).
[19] J.-P. Berenger, *J. Comp. Phys.* **114**, 185 (1994).
[20] M. Vallone, *et al.*, *J. Electron. Mater.* **45**, 4524 (2016).
[21] A. Tibaldi, *et al.*, *Opt. Express* **28**, 29253 (2020).
[22] M. Vallone, *et al.*, *IEEE J. Select. Topics Quantum Electron.*, DOI: 10.1109/JSTQE.2021.3056056.